Supporting information

Electrochemical in Situ Construction of Vanadium Oxide Heterostructures with Boosted Pseudocapacitive Charge Storage

Ran Dong, Yu Song*, Duo Yang, Hua-Yu Shi, Zengming Qin, Mingyue Zhang, Di Guo, Xiaoqi Sun, Xiao-Xia Liu*

Department of Chemistry, Northeastern University, Shenyang 110819, China

E-mail: songyu@mail.neu.edu.cn; xxliu@mail.neu.edu.cn

1. Calculations

1.1 Specific capacitance calculation based on galvanostatic charge/discharge curves

The gravimetric and areal capacitance of single electrodes is calculated based on Equation S1 and S2, respectively:

$$C_g = \frac{I \times t}{\Delta U \times m} \quad \text{(Equation S1)}$$

$$C_a = \frac{I \times t}{\Delta U \times S} \quad \text{(Equation S2)}$$

Where C_g and C_a are the gravimetric and areal specific capacitance (F/g or mF/cm^2), I is the current density (mA cm^{-2}), t is the discharge time (s), ΔU is the potential window (V), s is the geometric electrode working area (1 cm^2), and m represents the mass loading of the oxide on the electrode (mg cm^{-2}).

The gravimetric and areal capacitance of the device is calculated based on Equation S3 and S4, respectively:

$$C_G = \frac{I \times t}{U \times m} \quad \text{(Equation S3)}$$

$$C_A = \frac{I \times t}{U \times S} \quad \text{(Equation S4)}$$

Where C_G and C_A are the gravimetric and areal specific capacitance (F/g or mF/cm^2), U is the potential window of the device (V), s is the geometric device working area (1 cm^2), and m represents the mass loading of the oxide on the electrode (mg cm^{-2}).

The volumetric capacitance of the device from the constant current charge-discharge profile is calculated from Equation S5:

$$C_v = \frac{It}{VU} \qquad \text{(Equation S5)}$$

Where C_v is the volumetric capacitance of the device (F/cm^3), V is the volume of the device (cm^3).

1.2 Energy density and power density of the device

The gravimetric energy density (E, Wh/kg) and power density (P, W/kg) are calculated using the following two equations:

$$E_g = \frac{1000}{2 \times 3600} C_G U^2 \qquad \text{(Equation S6)}$$

$$P_g = \frac{3600 \times E_g}{t} \qquad \text{(Equation S7)}$$

Where C_G is the specific capacitance (F/g), U is the operating voltage (V) and t is the discharge time (s) measured in constant current charge/discharge experiments.

The areal energy density (E, mWh/cm^2) and power density (P, mW/cm^2) are calculated using the following two equations:

$$E_a = \frac{1000}{2 \times 3600} C_A U^2 \qquad \text{(Equation S8)}$$

$$P_a = \frac{3600 \times E_a}{t} \qquad \text{(Equation S9)}$$

Where C_A is the specific capacitance (F/cm^2), U is the operating voltage (V) and t is the discharge time (s) measured in constant current charge/discharge experiments.

The volumetric energy density (E, mWh/cm^3) and power density (P, mW/cm^3) are calculated using the following two equations:

$$E_v = \frac{1000}{2 \times 3600} C_v U^2 \qquad \text{(Equation S10)}$$

$$P_v = \frac{3600 \times E_v}{t} \qquad \text{(Equation S11)}$$

Where C_v is the specific capacitance (F/cm^3), U is the operating voltage (V) and t is the discharge time (s) measured in constant current charge/discharge experiments.

1.3 Charge balance for the device

To maximize the performance of a pseudocapacitor, the amount of charge (Q) stored in the anode and the cathode should be balanced, *i.e.* $Q_+ = Q_-$. The charge stored by each electrode depends on corresponding areal capacitance (C_a), their potential windows (ΔU) and the geometric working area of the electrode (S), as shown in the following equations:

$$Q_+ = C_{a,+} \times \Delta U_+ \times S_+ \qquad \text{(Equation S12)}$$

$$Q_- = C_{a,-} \times \Delta U_- \times S_- \qquad \text{(Equation S13)}$$

In order to get $Q_+ = Q_-$, the ratio of areal capacitance between the anode to the cathode should follow the following equation:

$$\frac{C_{a,-}}{C_{a,+}} = \frac{S_+ \times \Delta U_+}{S_- \times \Delta U_-} \qquad \text{(Equation S14)}$$

In this work, we chose V_5O_{12}/VO_2 and MnO_2 as the anode and cathode materials, respectively. Their working areas and potential windows were the same ($S_+ = S_-$, $U_+ = U_-$). According to Equation S14, the ratio of the areal capacitance of V_5O_{12}/VO_2 to the MnO_2 electrode is ~1, which is closed to the areal capacitance of V_5O_{12}/VO_2 (5.03 F cm^{-2}) to MnO_2 (5.0 F cm^{-2}) used in this work. The total mass of the active materials on both electrodes is ~23 mg cm^{-2}.

1.4 Computational method

All the calculations are performed in the framework of the density functional theory with the projector augmented plane-wave method, as implemented in the Vienna ab initio simulation package.[1] The generalized gradient approximation proposed by Perdew, Burke, and Ernzerhof is selected for the exchange-correlation potential.[2] The long-range van der Waals interaction is described by the DFT-D3 approach.[3] The cut-off energy for the plane wave is set to 400 eV. The energy criterion is set to 10^{-5} eV in the iterative solution of the Kohn-Sham equation. A vacuum layer of 15 Å is added perpendicular to the sheet to avoid artificial interaction between periodic images. The Brillouin zone integration is performed at the Gamma point. All the structures are relaxed until the residual forces on the atoms have declined to less than 0.03 eV/Å.

[1] Kresse, G.; Joubert, D. From ultrasoft pseudopotentials to the projector augmented-wave method. *Phys. Rev. B* **1999**, 59, 1758-177.

[2] Perdew, J. P.; Burke, K.; Ernzerhof, M. Generalized gradient approximation made simple. *Phys. Rev. Lett.* **1996**, 77, 3865-3868.

[3] Grimme S, Antony J, Ehrlich S, et al. A consistent and accurate ab initio parametrization of density functional dispersion correction (DFT-D) for the 94 elements H-Pu. *J. Chem. Phys.* **2010**, 132, 154104.

2. Supplementary Table

Table S1. Electrochemical performances of the state-of-the-art vanadium oxide electrodes compared with that of $V5O_{12}/VO_2$ electrode.

Sample	*Gravimetric Capacitance ($F\ g^{-1}$)*	*Areal Capacitance ($mF\ cm^{-2}$)*	*Current Density/ Scan rate*	*Potential Window (V)*	*Mass Loading ($mg\ cm^{-2}$)*
Ti-VOx-CNT[1]	310	341	2 mV s^{-1}	-1~0.8 vs.A	1.1
VOx/graphene[2]	358	716	0.5 mA cm^{-2}	-0.2~0.8 vs.SCE	2.0
VOx[3]	637	356.8	0.5 mA cm^{-2}	0~0.8 vs.SCE	0.56
S-V_6O_{13-X}[4]	1353	720	1.0 mA cm^{-2}	-1~0 vs.SCE	0.52
VOx-PANI[5]	443	664	0.5 mA cm^{-2}	-0.9~0.7 vs.SCE	1.5
V_2O_5-carbonfiber[6]	408	856.8	2.1 mA cm^{-2}	-0.3~0.7 vs.SCE	2.1
VOx-carbonfiber[7]	485	1310	1 mA cm^{-2}	-1.1~0.9 vs.SCE	2.7
V_2O_5-PPy[8]	412	206	4.5 mA cm^{-2}	-1.4~0.6 vs.SCE	~0.5
V_2O_5[9]	735	400	1 mV s^{-1}	0~1 vs. A	0.54
V_2O_5-RGO[10]	178.5	382	0.05 A g^{-1}	-0.8~0.8 vs. A	2.2
V_5O_{12}/VO_2	**466**	**5032**	**1 mA cm^{-2}**	**-1~0 vs. SCE**	**~10.8**

*A : Ag/AgCl

[1] P. H. Jampani, O. Velikokhatnyi, K. Kadakia, D. H. Hong, S. S. Damle, J. A. Poston, A. Manivannan, P. N. Kumta, *J. Mater. Chem. A* **2015**, *3*, 8413-8432.

[2] L. Deng, Y. Gao, Z. Ma, G. Fan, *J. Colloid Interface Sci.* **2017**, *505*, 556-565.

[3] M. Yu, Y. Zeng, Y. Han, X. Cheng, W. Zhao, C. Liang, Y. Tong, H. Tang, X. Lu, *Adv. Funct. Mater.* **2015**, *25*, 3534-3540.

[4] T. Zhai, X. Lu, Y. Ling, M. Yu, G. Wang, T. Liu, C. Liang, Y. Tong, Y. Li, *Adv. Mater.* **2014**, *26*, 5869-5875.

[5] M.-H. Bai, T.-Y. Liu, F. Luan, Y. Li, X.-X. Liu, *J. Mater. Chem. A* **2014**, *2*, 10882-10888.

[6] L. Li, S. Peng, H. B. Wu, L. Yu, S. Madhavi, X. W. D. Lou, *Adv. Energy Mater.* **2015**, *5*, 1500753.

[7] Z.-H. Huang, Y. Song, X.-X. Liu, *Chem. Eng. J.* **2019**, *358*, 1529-1538.

[8] M. H. Bai, L. J. Bian, Y. Song, X. X. Liu, *ACS Appl. Mater. Interfaces* **2014**, *6*, 12656-12664.

[9] B. Pandit, D. P. Dubal, B. R. Sankapal, *Electrochim. Acta* **2017**, *242*, 382-389.

[10] C. Y. Foo, A. Sumboja, D. J. H. Tan, J. Wang, P. S. Lee, *Adv. Energy Mater.* **2014**, *4,* 1400236.

3. Supplementary figures

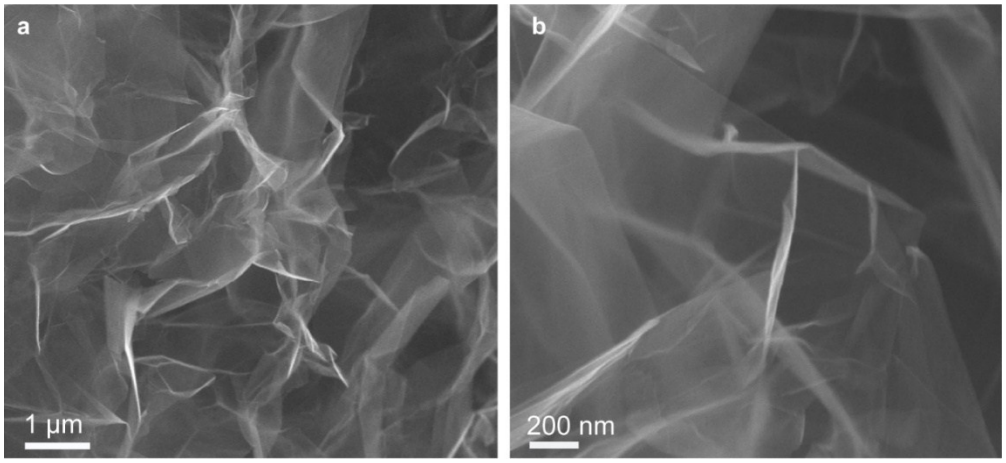

Figure S1 SEM images for the exfoliated graphite paper electrode (EG).

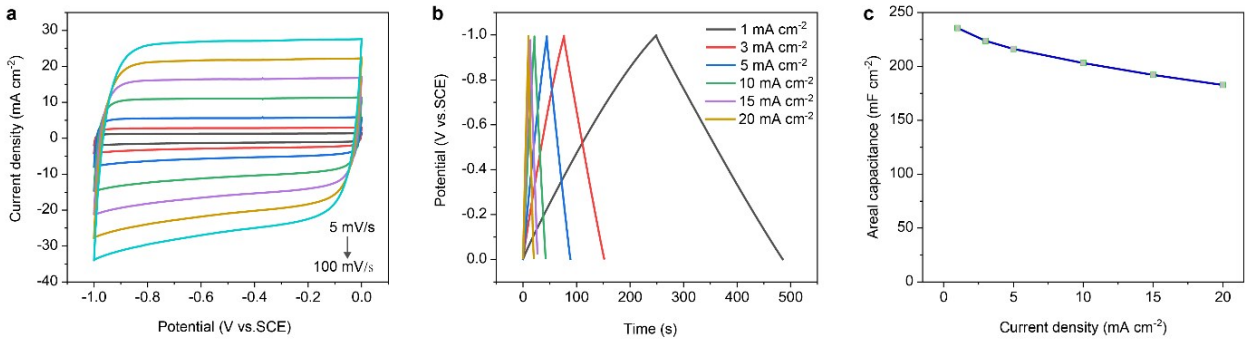

Figure S2 Electrochemical performances of the EG substrate. (a) CV curves, (b) galvanostatic charge/discharge curves, (c) rate capability. The rectangular CV and symmetric charge/discharge curves indicate the ideal capacitive performance of the EC substrate.

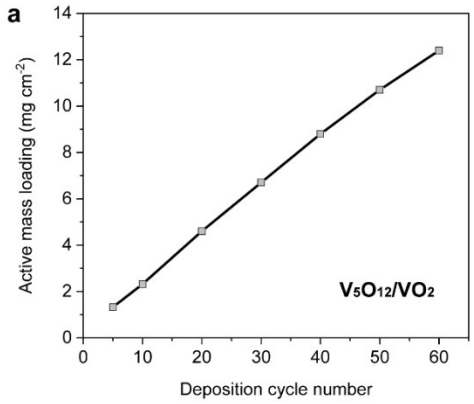

Figure S3 Active mass loading of V_5O_{12}/VO_2 as a function of deposition cycle number.

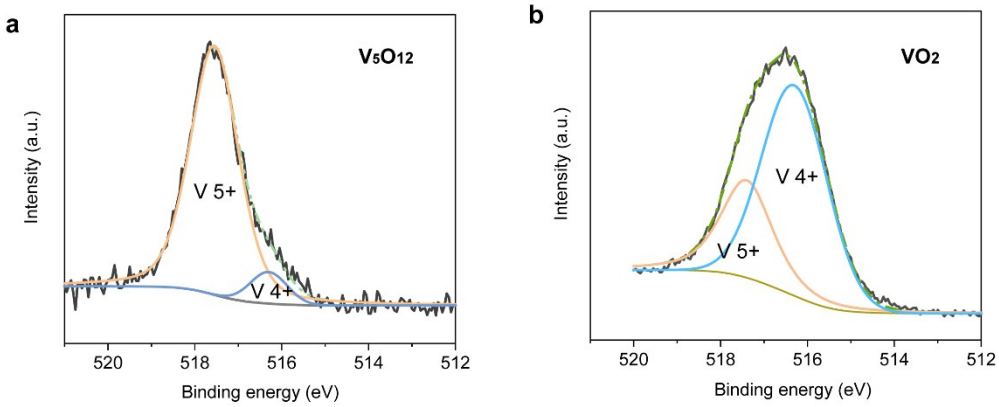

Figure S4 XPS V 2p core-level spectra of (a) V_5O_{12} and (b) VO_2 samples. The average valence states of V in pure V_5O_{12} and VO_2 electrodes were calculated to be ~ +4.9 and +4.3, respectively (Figure S4). The slightly higher valence states of V than the stoichiometric values in the samples could be due to the surface oxidation of V in the atmosphere.

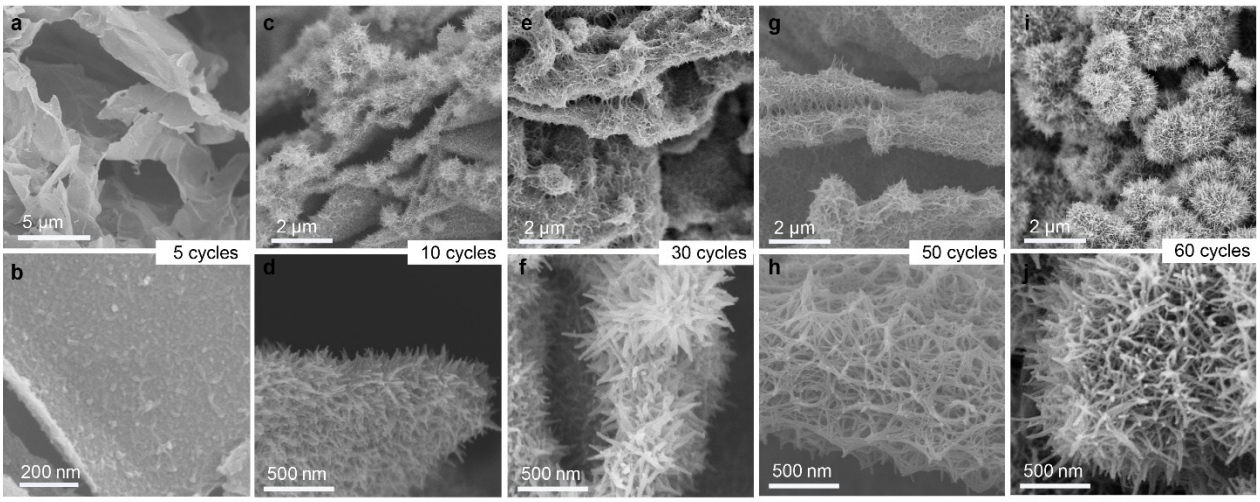

Figure S5 SEM images of the vanadium oxides deposited on EG obtained from different CV cycles. (a, b) 5 cycles; (c, d) 10 cycles; (e, f) 30 cycles; (g, h) 50 cycles; (i, j) 60 cycles.

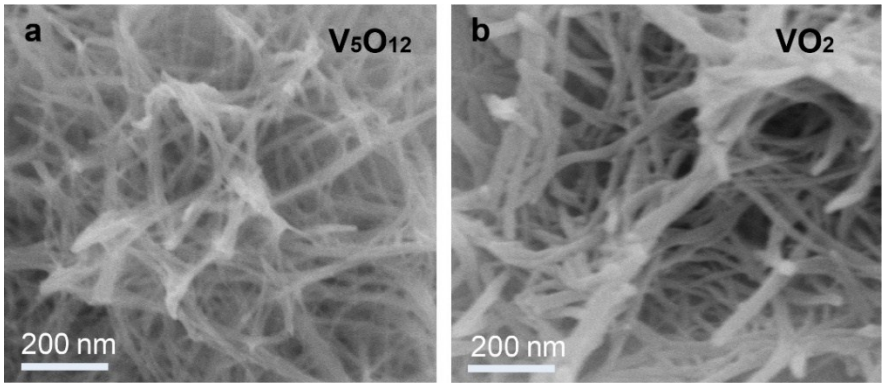

Figure S6 SEM images of V_5O_{12} and VO_2.

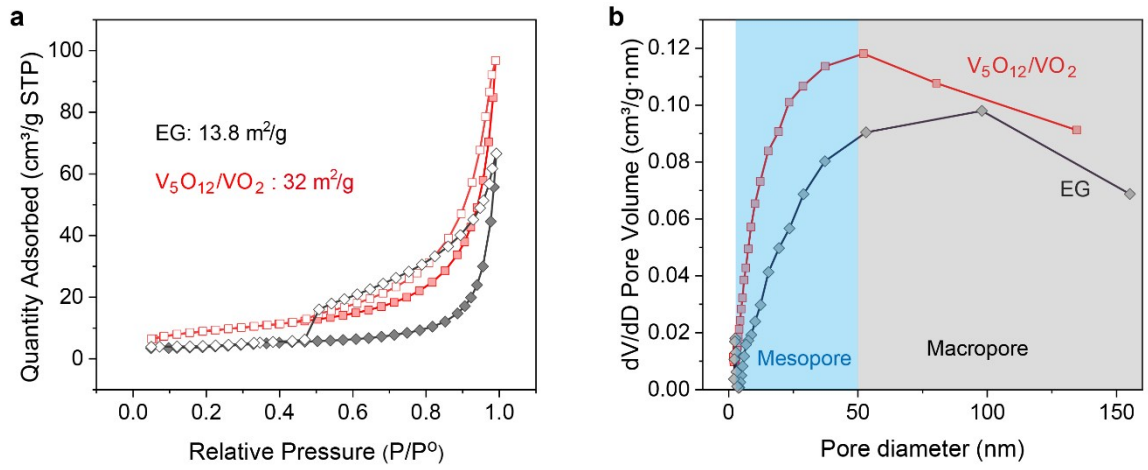

Figure S7 (a) N_2 adsorption-desorption isotherms of V_5O_{12}/VO_2 and EG electrodes collected at 77 K. (b) The pore size distribution of the electrodes derived from the adsorption curves using BJH theory.

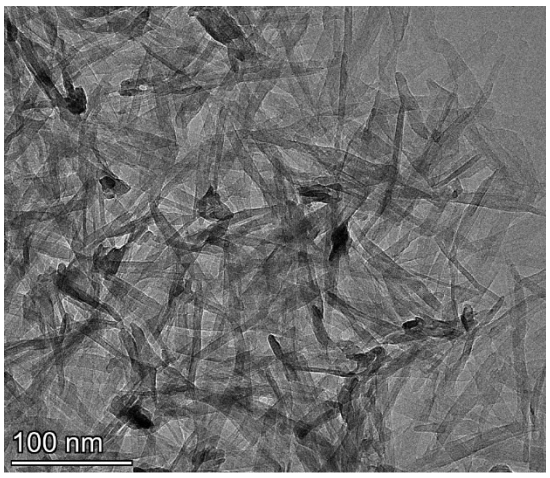

Figure S8 TEM image of V_5O_{12}/VO_2 composite

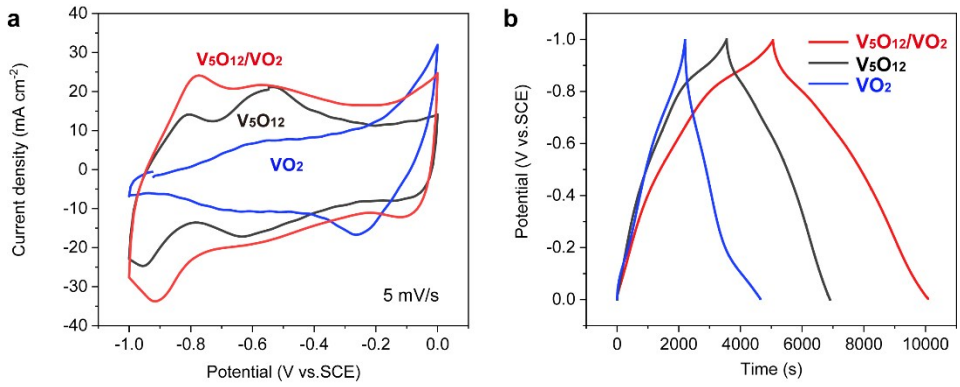

Figure S9 (a) CV and (b) galvanostatic charge/discharge curves of V_5O_{12}/VO_2, V_5O_{12}, and VO_2 electrodes.

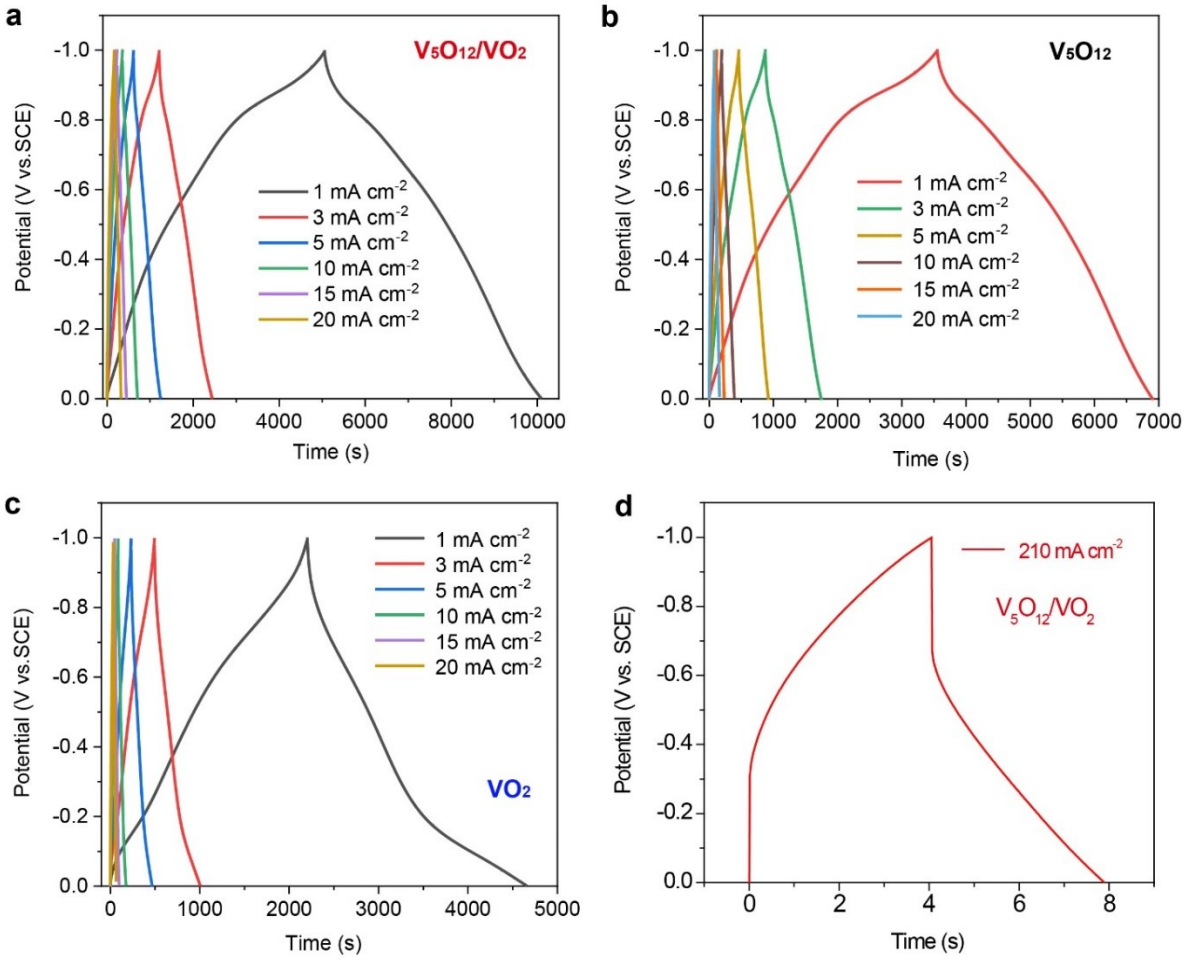

Figure S10 Galvanostatic charge/discharge curves of (a) V_5O_{12}/VO_2, (b) V_5O_{12}, and (c) VO_2 electrodes. (d) Charge/discharge curve of V_5O_{12}/VO_2 at the current density of 210 mA cm^{-2}.

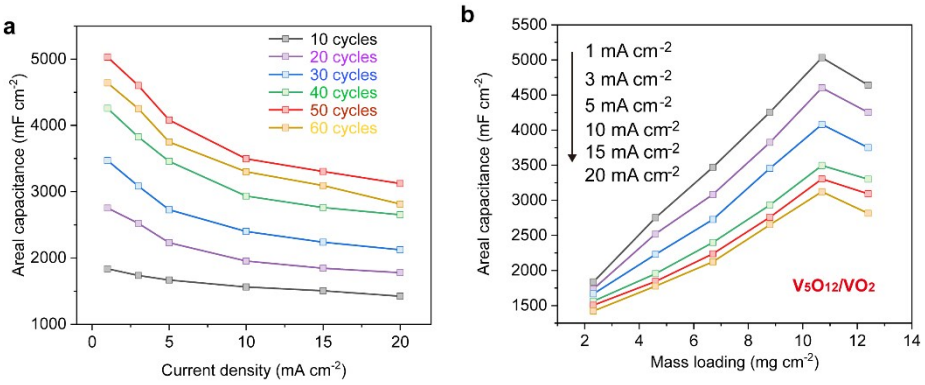

Figure S11 (a) Areal capacitance as a function of the current density of the V_5O_{12}/VO_2 materials deposited with different cycles. (b) Areal capacitance as a function of mass loading of the V_5O_{12}/VO_2 materials at different current densities.

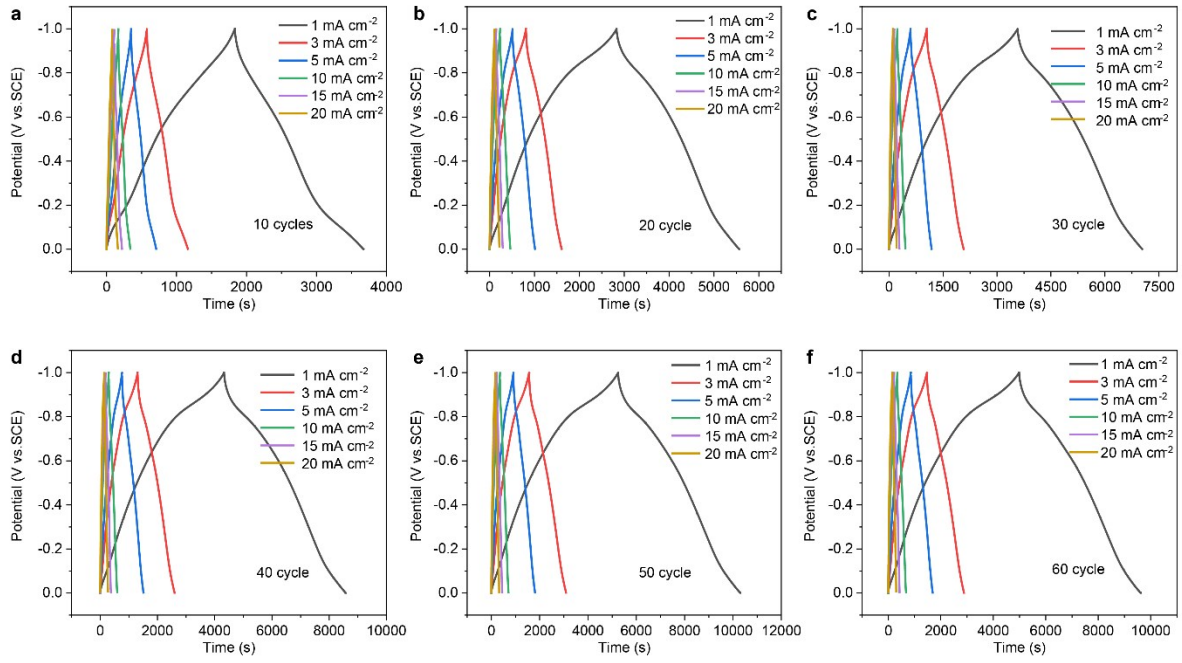

Figure S12 Galvanostatic charge/discharge curves of the V_5O_{12}/VO_2 materials deposited with different cycles.

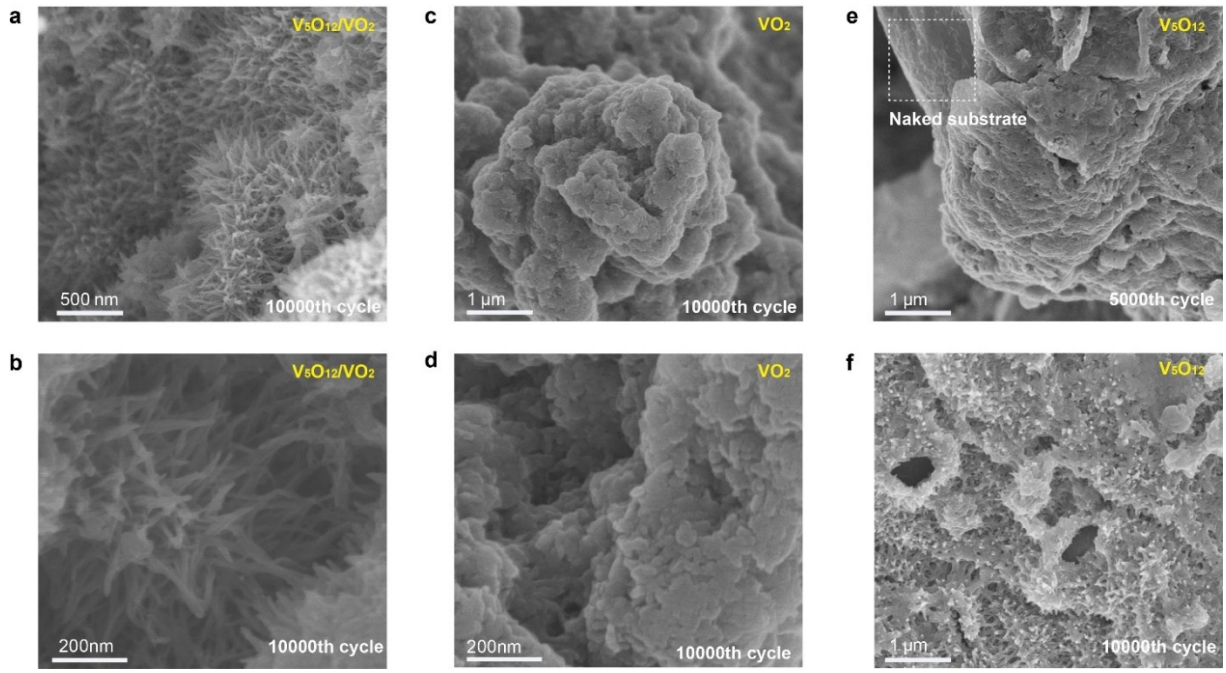

Figure S13 (a, b) SEM images of the V_5O_{12}/VO_2 electrode after 10000 charge and discharge cycles. (c, d) SEM images of the VO_2 electrode after 10000 charge and discharge cycles. (e) SEM image of the V_5O_{12} electrode after 5000 charge and discharge cycles. (f) SEM images of the V_5O_{12} electrode after 10000 charge and discharge cycles.

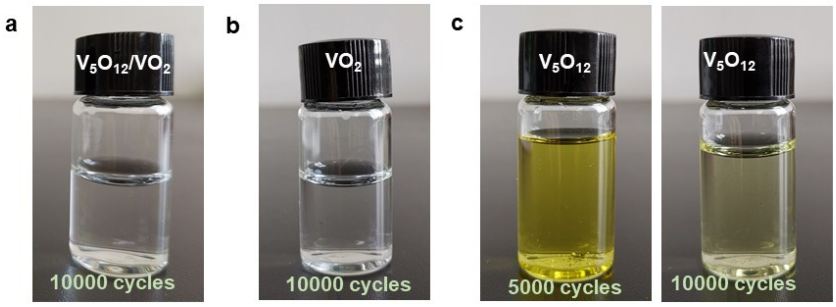

Figure S14 (a) The digital photograph of the electrolyte after 10000 charge and discharge cycles for the V_5O_{12}/VO_2 electrode. (b) The digital photograph of the electrolyte after 10000 charge and discharge cycles for the VO_2 electrode. (c) The digital photographs of the electrolyte after 5000 and 10000 charge and discharge cycles for the V_5O_{12} electrode.

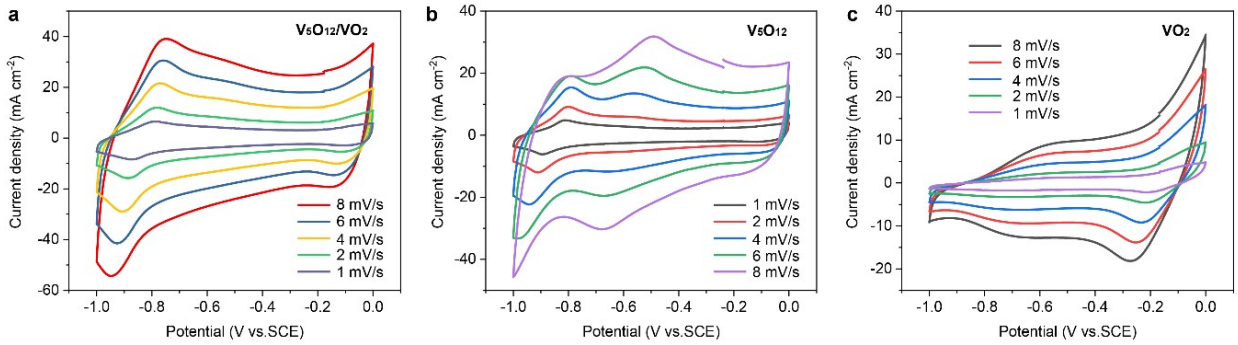

Figure S15 CV curves of (a) V_5O_{12}/VO_2, (b) V_5O_{12} and (c) VO_2 from 1 to 8 mV s^{-1}.

Dunn Method:

According to the Dunn method, the current response at a fixed potential comes from two separate mechanisms, capacitive-controlled and diffusion-controlled processes:

$$i(\mathrm{V}) = k_1 v + k_2 v^{1/2} \qquad \text{(Equation 15)}$$

Where $k_1 v$ is the current contribution from the capacitive effect, and $k_2 v^{1/2}$ corresponds to the current contribution from the diffusion-controlled process. Dividing $v^{1/2}$ on both sides of the equation gives:

$$i(\mathrm{V})/v^{1/2} = k_1 v^{1/2} + k_2 \qquad \text{(Equation 16)}$$

By reading the i(V) at a selected potential from CV curves collected at different scan rates followed by plotting i(V)/$v^{1/2}$ *vs.* $v^{1/2}$, in the linear fitting line, k_1 equals the slope and k_2 equals the y-intercept. Using the k_1 and k_2 obtained above, current contributions from the capacitive effect ($k_1 v$) and diffusion-controlled process ($k_2 v$) at the specific potential are obtained according to Equation (15).

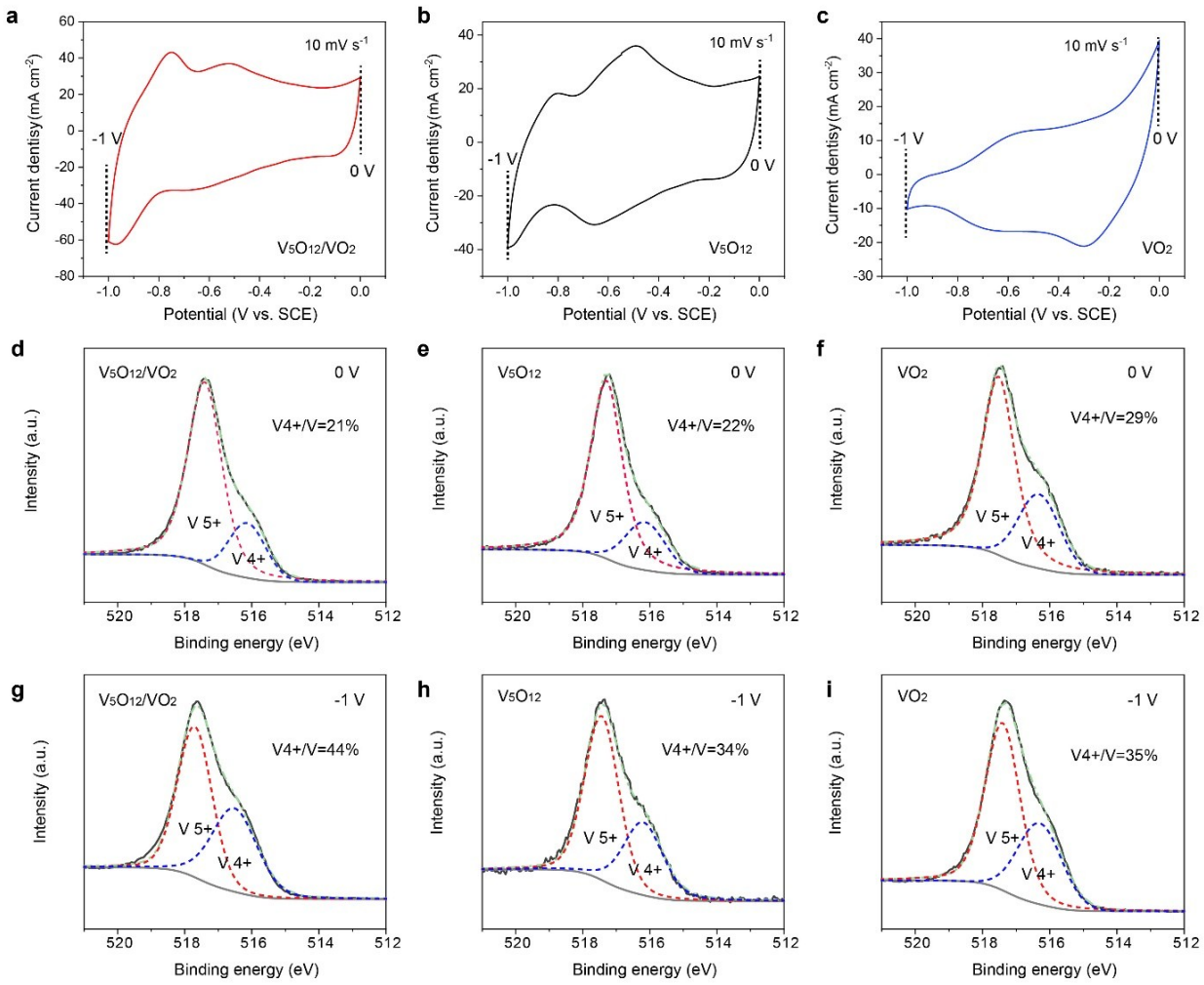

Figure S16 CV curves of (a) V_5O_{12}/VO_2, (b) V_5O_{12} and (c) VO_2 at the scan rate of 10 mV s^{-1}. XPS core-level V 2p spectra of (d) V_5O_{12}/VO_2, (e) V_5O_{12} and (f) VO_2 collected at ~ 0 V *vs*. SCE; XPS core-level V 2p spectra of (g) V_5O_{12}/VO_2, (h) V_5O_{12} and (i) VO_2 collected at ~ −1 V *vs*. SCE. The V^{4+}/V (*i.e.* $V^{4+} + V^{5+}$) ratios based on the areal of the fitting peaks were denoted in the figures.

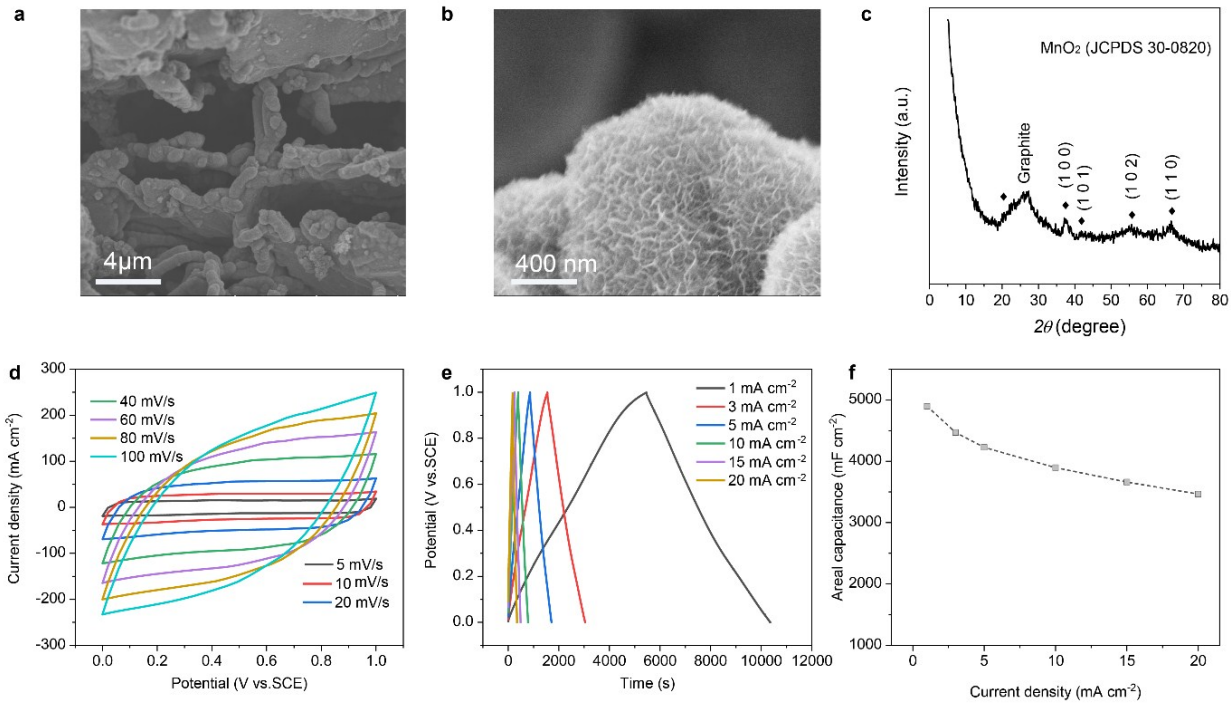

Figure S17 (a, b) SEM images of the MnO_2 materials deposited on a 3D exfoliated graphite (EG) substrate. MnO_2 nanosheets were uniformly deposited on the exfoliated graphite/graphene sheets. (c) XRD pattern of the MnO_2/EG electrode. The XRD pattern of the sample matches well with the standard pattern of hexagonal ε-MnO_2 (JCPDS 30-0820). (d) CV curves of the MnO_2/EG electrode at different scan rates. (e) Galvanostatic charge/discharge curves of the MnO_2/EG electrode. (f) Rate performance of the MnO_2/EG electrode. The MnO_2/EG electrode (~12 mg cm^{-2}) exhibits a good real capacitance of 4.90 F cm^{-2} at the current density of 1 mA cm^{-2}.

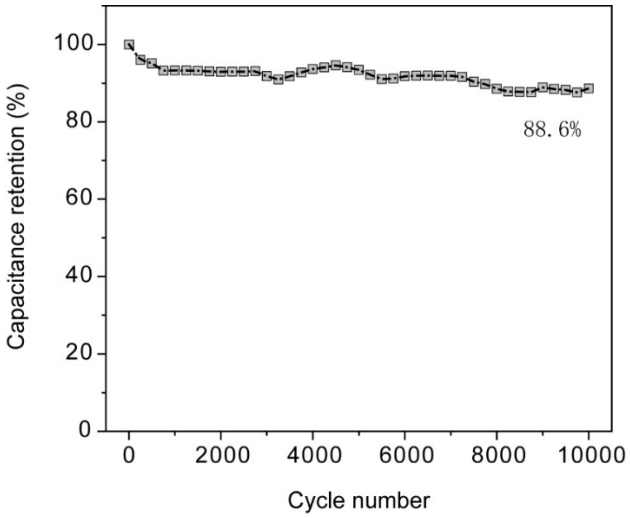

Figure S18 Cycling stability of the device.